Perturbational Treatment of the Gravitational Potential Effect on Binary Black Hole Evolution

Zhoujian Cao*,[1] Jui-Ping Yu,[2] Chun-Yu Lin,[2] Shan Bai,[3] and Hwei-Jang Yo†[4]

[1] *Institute of Applied Mathematics, Academy of Mathematics and Systems Science, Chinese Academy of Sciences, Beijing 100190, China*

[2] *Department of Physics and National Center for Theoretical Sciences, National Cheng-Kung University, Tainan 701, Taiwan*

[3] *Institut de Mathématiques de Bourgogne, Université de Bourgogne, 9 avenue Alain Savary, 21078 Dijon Cedex, France*

[4] *Department of Physics, National Cheng-Kung University, Tainan 701, Taiwan*

(Dated: March 1, 2013)

Binary black hole (BBH) systems are usually located in the gravitational potential well formed by a massive black hole (BH), which is mostly located in the center of a galaxy. In most existing studies, the BBH systems are treated as isolated systems, while the effect of the background is ignored. The validity of the approximation is based on the belief that the background gravitational field from other sources is extremely weak compared with the strong gravitational field produced by the BBH itself during the evolution, and can be neglected in gravitational wave detection. However, it is still interesting to check how valid this approximation is. In this work, instead of simulating the three-BH problem with a fully relativistic treatment, we use a perturbational scheme to investigate the effect of the background gravitational potential on the evolution of a BBH, especially on the waveform of its gravitational radiation. Four scenarios are considered including the head-on collision and the inspiral-to-merger process of a BBH which is either freefalling towards or circularly orbiting around a third large BH. The head-on collision and the circular inspiral are two limits of all possible configurations. The existence of the background gravitational potential changes the arrival time of the gravitational wavefront of a BBH, prolongs the wavelength, and increases the gravitational radiation energy. And most interestingly, the background gravitational potential induces the higher-order modes of the gravitational wave of a BBH. These interesting phenomena can be explained by the gravitational redshift effect and the change of eccentricity of a BBH's orbit from the background gravitational potential. Without further studies, these phenomena could introduce complications or even mislead people in the identification of the source of gravitational wave and in distinguishing the signatures of an isolated BBH from a BBH in a background gravitational potential.

PACS numbers: 04.25.Dm, 04.30.Db, 95.30.Sf, 97.60.Lf

I. INTRODUCTION

In numerical relativity, Einstein's equation can be solved numerically without any approximation or symmetry assumption, with the aid of a supercomputer. Besides the massive computational cost involved, the stability issue is also a nontrivial problem in the numerical calculations for Einstein's equation. Breakthroughs in 2005 and 2006 [1–3] shifted the development of numerical relativity to a higher pace. Now many numerical relativity groups around the world are capable of evolving black hole (BH) systems with high accuracy. Moreover, a variety of interesting topics, such as long term gravitational waves [4–14], gravitational radiation induced BH recoil [15–30], the estimation of the final BH's mass and the spin of binary black hole systems [31–36], and so on [37–42], have been extensively studied over the past few years. Numerical relativity has now become an efficient tool in the research of general relativity and astrophysics.

Gravitational wave detection is an important task for the further development of gravitation and general relativity. Currently, the ground-based laser interferometers such as LIGO [43], VIRGO [44], GEO600 [45], and TAMA [46] are already up and running, while the space-based laser interferometer LISA [47] is still under construction. Progress in detection has made the requirement for the theoretical prediction of gravitational wave signal more and more urgent. Numerical relativity plays a key role in both aiding gravitational wave data analysis [48] and helping to build template banks of the phenomenological waveform [49] for the most important gravitational source—binary black hole (BBH) coalescence.

In most theoretical and numerical calculations, BBHs are treated as isolated systems, although stellar-mass BBHs usually are located in a galaxy with a super-massive BH in the center. The validity of the approximation is based on the idea that a stellar-mass BBH is usually far away from the super-massive BH whose gravitational potential is negligible compared with the strength of the gravitational field produced by the BBH itself. Besides the possible super-massive-BH environment, it is possible for stellar-mass BBHs to be affected

*zjcao@amt.ac.cn
†hjyo@phys.ncku.edu.tw

by other stellar BHs and/or stars, especially in globular clusters. Although the background potentials in these scenarios are usually much weaker than the gravitational field of the BBH, it still remains as an interesting question as to how valid the approximation is, and to what extent the approximation holds. There have been several studies of the three-BH problem with numerical relativity from various standpoints [37, 38, 50–53]. The results all indicate that the dynamics and behavior displayed by three BHs are qualitatively different from those of an isolated BBH. For example, in [50], numerically generated BBH initial data sets and post-Newtonian techniques are utilized to show that the presence of a third BH has non-negligible relativistic effects on the location of a BBH's innermost stable circular orbit (ISCO), an increase in merging time, and an amplification of the gravitational radiation emitted from the BBH. As we all know, information about a BBH such as the initial/final spin, the mass ratio and the orientation can be extracted from a detected gravitational wave by comparing the wave train with the waveform template in the data bank calculated with theoretical models. Without proper consideration of the environmental effect on the BBH evolution and thus on the distortion of the gravitational wave, the extracted information might be incorrect and possibly lead to misinterpretation and/or misunderstanding. It is also possible that the nonlinearity of general relativity might give rise to a qualitatively difference due to a tiny difference, just like in other nonlinear systems [54]. It is also interesting to seek any possible nonlinear effects in the three-BH problem which might be helpful in distinguishing among different scenarios [55].

In this work, instead of the heavily numerical calculation of the evolution of a three-BH problem with a fully relativistic treatment, we use a perturbational scheme, along with numerical simulations, to investigate the effect of the background gravitational potential on the evolution of a BBH, especially on the waveform of the gravitational radiation. As with our previously preliminary study [56], the scenarios we considered include the head-on collision and the inspiral-to-merger process of a BBH, considered as the two limits in all possible configurations, in the cases where the BBH is freefalling towards or circularly orbiting around the third large BH. Our results show that the existence of the background gravitational potential changes the arrival time of the gravitational wavefront of the BBH, prolongs the wavelength, and increases the gravitational radiation energy. And most interestingly, the background gravitational potential induces the higher-order modes of the gravitational wave of a BBH. These interesting phenomena can be explained by the gravitational redshift effect and the change of eccentricity of the BBH's orbit from the gravitational potential. These phenomena could introduce complications or even mislead people in the identification of the source of gravitational wave without further studies to distinguish the signatures of a BBH with a background gravitational potential from the ones of an isolated BBH.

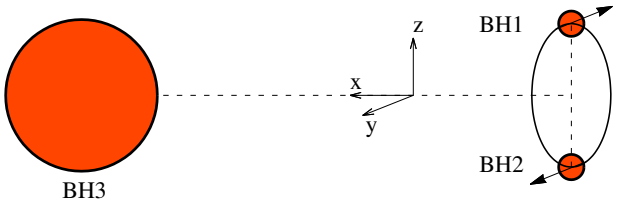

FIG. 1: A schematic illustration of a BBH system in the gravitational potential of a third massive BH.

The remainder of the paper is organized as follows: In Sec. II, we give a description of the code configuration, the gauge condition, the initial data, and especially the perturbational method for the outer boundary condition. Then we consider the four special cases for the evolution of a BBH under the influence of a third large BH, followed by a numerical analysis of these results one by one in Sec. III. We summarize and discuss the viability of the perturbational method and the implications of our findings in Sec. IV. Throughout the paper, the geometric units with $G = c = 1$ are used.

II. NUMERICAL TECHNIQUES

As a preliminary study of the background effect, we investigate the dynamics and the waveforms of a BBH system in a potential background which comes from a third, distant and massive BH. For this three-body system, we do not simulate its three-body dynamics with a fully relativistic treatment as in [53]. Instead, a method of perturbation is adopted for the problem since the gravitational field from the third BH to the BBH is weaker than the field between the two small BHs in the BBH. It is obvious that the effect of the third massive BH is stronger if it has larger mass m_3 or the shorter distance R to the binary system, or both. Therefore, we would use the ratio of m_3/R to denote the strength of the gravitational background resulting from the third massive BH. Figure 1 illustrates the configuration considered in this work.

A. Code configuration and Gauge condition

Our AMSS-NCKU code for solving Einstein's field equations based on the BSSN formalism is updated from our previous work [57]. For the time integration, we updated from the iterative second-order Crank-Nicholson method to the fourth-order Runge-Kutta method. We also developed our own infrastructure for the implementation of the fixed mesh refinement and its parallelization in addition to using the GrACE package [58]. Our new infrastructure also provides a "moving box" style mesh refinement. The box will move to follow the position of

the BHs, which are determined by [2]

$$\frac{\mathrm{d}}{\mathrm{d}t}x^i_{BH} = -\beta^i(x^i_{BH}). \tag{1}$$

We follow closely [59, 60] in the development of the new infrastructure to deal with the interface between two mesh levels. Since three time levels are used for the interpolation in time, we adopt the scheme described in [61] to prepare the initial data. With GrACE, the time step for every mesh level is set to be that the Courant factor times the finest spatial resolution. However, with our new infrastructure, the time step is set by following the recipe in [59, 60]. Typically, the Courant factor is set between 0.25 and 0.5. The results obtained with our infrastructure and with GrACE's fixed mesh refinement are consistent with each other.

The choice of gauge condition is essential for a long-term stability in the numerical evolution to avoid the encounter of singularity and large spatial coordinate stretch. The "1+log" condition for the lapse [62] and the Γ-driver condition for the shift [63], which are called "the moving puncture gauge" together, have been successfully applied to the long-term stable BBH simulations based on the BSSN formulation [2, 3]. In [57], we have reviewed and studied the parameters and the additional advection terms for this type of gauge condition used in the community. Therefore, in this work, we adopt

$$\partial_t\alpha - \lambda_1\beta^j\partial_j\alpha = -2\alpha K, \tag{2}$$

$$\partial_t\beta^i - \lambda_2\beta^j\partial_j\beta^i = \frac{3}{4}f(\alpha)B^i, \tag{3}$$

$$\partial_t B^i - \lambda_3\beta^j\partial_j B^i = \partial_t\tilde{\Gamma}^i - \lambda_4\beta^j\partial_j\tilde{\Gamma}^i - \eta B^i, \tag{4}$$

where $(f(\alpha), \eta, \lambda_1, \lambda_2, \lambda_3, \lambda_4) = (\alpha, 2, 1, 1, 1, 1)$. The initial gauge conditions are chosen as $\alpha = \psi^{-2}$, $\beta^i = 0$, and $B^i = 0$. It has been confirmed in [57] that this configuration allows stable evolutions.

B. Multi-puncture initial data with spectral method

In this section, we review the puncture scheme and then describe how the multi-puncture BH initial data is constructed by the multi-domain spectral method extended from the LORENE library [64, 65]. Here we emphasize that our initial data for the three-BH problem is from the numerical calculation solving the full Einstein constraint equations.

With the assumption of conformal flatness and maximal slicing in the conformal decomposition of the $3+1$ formalism of general relativity (see [66] for instance), the constraint equations are greatly simplified and also decoupled. And thus the momentum constraint allows the Bowen-York solution [67] for the conformally trace-free part of the extrinsic curvature of each hole,

$$\hat{A}^{ij}_a \equiv \psi^{10}A^{ij}_a = \frac{3}{4r^2}[P^{(i}n^{j)} - 2(\gamma^{ij} - n^in^j)P_kn^k] + \frac{3}{2r^3}n^{(i}\epsilon^{j)k\ell}S_kn_\ell, \tag{5}$$

where $\vec{n}$ is the spatial unit vector pointing away from the puncture, and $\vec{P}$ and $\vec{S}$ correspond respectively to the linear momentum and the intrinsic angular momentum of each hole. $\hat{A}^{ij}$ can be linearly superposed for multi-hole spacetime with $\hat{A}^{ij} = \sum_{a=1}^{N}\hat{A}^{ij}_a$ since the momentum constraint equation is linear in this case. The conformal factor then can be solved from the Hamiltonian constraint as

$$\tilde{D}^2\psi = -\frac{1}{8}\psi^{-7}\hat{A}_{ij}\hat{A}^{ij}. \tag{6}$$

To deal with the physical singularity of the BH, one separates out the singular part

$$\psi_s = 1 + \frac{1}{2}\sum_a\frac{m_a}{r_a}, \tag{7}$$

from the conformal factor ψ, where m_a is the mass parameter for each puncture and r_a is the coordinate distance from each puncture. Equation (7) is the exact multi-hole solution at rest satisfying the flat Laplacian equation [68]. The desired regular part $u \equiv \psi - \psi_s$ satisfies the elliptic equation

$$\tilde{D}^2u = -\frac{1}{8}\hat{A}^{ij}\hat{A}_{ij}(\psi_s + u)^{-7}. \tag{8}$$

The existence and uniqueness of the solution has been discussed in [69].

Solving elliptic equations is computationally expensive. The spectral method is emphatically suitable to be applied to it for its high precision and fast convergence, provided the solution is a smooth function. The spectral method has been successfully applied to study the relativistic star model [70]. And the LORENE library has been developed to provide a multi-shell domain framework for this type of problem. For the puncture initial data, due to the at most $\mathcal{C}^2$ property of u at the puncture as discussed in [69], the direct application of the spectral method would only give a polynomial convergence. The two-puncture data with spectral method was first extensively studied in [71] with a series of coordinate transformations which modify and improve the order of smoothness of the solution in the new coordinate. This scheme has been widely used in the numerical relativity community, though it is not easy to be generalized to a multi-puncture scenario. The multi-puncture data was studied recently with a multi-grid method in [52].

Our multi-puncture initial data solver is motivated by the earlier work [72] for the excised BBH initial data. In this code we cover on each BH a spherical multi-shell

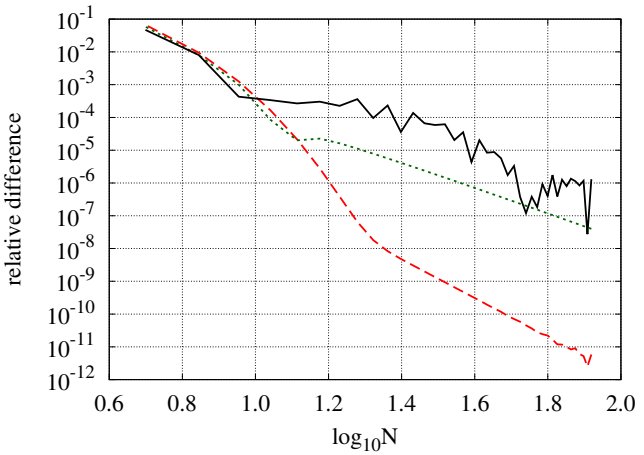

FIG. 2: Local convergence test (at the puncture) for the initial data of a single boosted BH (dashed-red) with $P = 0.2$, a spinning BH (dotted green) with $S = 0.2$, and an equal-mass BBH (solid) separated by $6M$ with $P = \pm 0.2$, respectively. The vertical axis indicates the relative difference between the solution u at $N_r = N$ and the one at the next higher resolution. For the single BH cases, the angular resolution $(N_\theta, N_\phi) = (N_r, 4)$ which provides sufficient polar angular resolution for this axisymmetric test. For the BBH case, $(N_\theta, N_\phi) = (13, 16)$. Both of them displays exponential convergence at lower resolution and polynomial convergence after the difference has dropped below certain value which is dependent on the choice of domain boundaries.

domain, and split $u = \sum_a u_a$ (the index a runs over the number of the BHs) and the puncture equation (8) into

$$\tilde{D}^2 u_a = -\frac{1}{8}\hat{A}_a^{ij}\hat{A}_{ij}(\psi_s + u)^{-7}. \tag{9}$$

Note that only one of the extrinsic curvature tensors is split in the equation. Therefore, the source term in the RHS contributes only near each hole. The use of spherical polar coordinates is adequate for solving the equation near the punctures. Both $\hat{A}_{ij}$ and ψ_s are known analytically and would be set once and for all in the source term. The value of u_a is imposed to be zero at the physical outer boundary (at infinity) on the outermost, compactified shell. And $\partial_r u_a(r = 0) = 0$ is also ensured at the punctures as the inner boundary condition. These equations for each hole are then solved iteratively with the Poisson solver in the LORENE library until each successive difference of δu_a is as small as possible, typically 10^{-11}. In the three-BH scenario, the massive hole is fixed and offers a fixed gravitational potential background, therefore there is only two Poisson equations that need to be solved in each iteration. We have also checked the resulting data and found that it is very close to the one from the superposition of the solution of the small binary and the solution of the third massive BH. This is expected since the massive BH in our study is distant to the binary.

The convergence tests shown in Fig. 2 for a single boosted BH, a spinning BH, and a BBH display a rapid convergence to a high precision. It is clear that the convergence is exponential with low resolution, but turns to be polynomial with high resolution, as expected in [73]. The turning point from an exponential convergence to a polynomial convergence mainly depends on the choice of the domain boundaries, as well as the order of the solution's smoothness. However, it is also known that the polynomial convergence at higher resolution depends only on the singular structure of the solution.

The momentum parameter for the quasi-circular binary is set according to the fitting curve based on the helical Killing vector conditions in [74]. As we note that, in the puncture scheme, only the metric of 3-geometry was specified, while the initial lapse and shift are chosen as the moving puncture gauge condition described in the beginning of this section. Nevertheless, it is justified in our experience that the choice of initial gauge for the puncture data has little effect on the resulting physical content, at least within our numerical accuracy.

C. Boundary condition

In numerical relativity the Sommerfeld radiation boundary condition is widely used and also a good approximation for no reflection from the boundary at a finite distance. For our BBH simulation with a time-independent gravitational background, the field variable set $Q(t, r) = \{\phi, \tilde{\gamma}_{ij} - \eta_{ij}, K, \tilde{A}_{ij}, \tilde{\Gamma}^i\}$ receives the gravitational contribution from the BBH and from the third large BH respectively as

$$Q(t, r) = Q_{\rm BBH}(t, r) + Q_{\rm 3rd}(r), \tag{10}$$

where the first term $Q_{\rm BBH}$ in the RHS includes the dynamical outgoing wave, while the second term $Q_{\rm 3rd}$ in the RHS serves as a fixed gravitational background which are trivially zero except the conformal factor of the third BH,

$$\phi_{\rm 3rd} = \ln\left(1 + \frac{m_3}{2|\vec{r} - \vec{r}_3|}\right). \tag{11}$$

In order to update the variable set $Q(t, r)$ at the outer boundary, we first extract $Q_{\rm BBH}(t_0, r)$ at the current time step t_0 by subtracting from $Q(t_0, r)$ the $Q_{\rm 3rd}(r)$ which is fixed in the whole evolution. Then, as usual, the Sommerfeld boundary condition is applied [75] to obtain the numerical data of $Q_{\rm BBH}(t_1, r)$ on the outer boundary for the next time step t_1. And finally we add $Q_{\rm 3rd}(r)$ back to the new $Q_{\rm BBH}(t_1, r)$ to obtain $Q(t_1, r)$. For the gauge variables, we use the usual Sommerfeld boundary condition for stability.

To justify the appropriateness of the modified boundary condition, we have performed two simulations with different outer boundaries and found their difference on the trajectory and gravitational waveform of the BBH are ignorable, as shown in Fig. 16 (Further details are explained in Sec. III D). Therefore, our boundary condition does not introduce unphysical drift to the BBH and

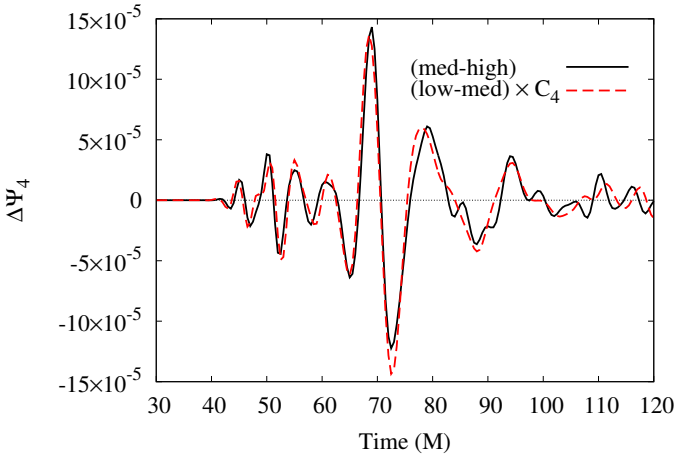

FIG. 3: Fourth-order convergence of the waveforms for the head-on collisions of an isolated BBH system. The solid line represents the difference of Ψ_4 between the high and medium resolutions. The red-dashed line represents the difference between the medium and low resolutions with a convergence factor C_4.

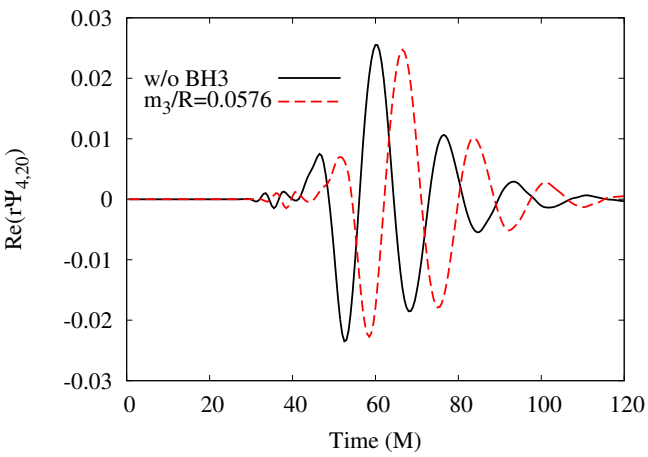

FIG. 4: The typical waveforms for the head-on collisions of an isolated BBH and for the head-on-freefall case in Sec. III A. The red-dashed (black-solid) line represents the case with (without) the third BH. The $(\ell = 2, m = 0)$ mode of Ψ_4 detected at $r = 40$ is plotted. The gravitational potential of the third BH causes mainly shifts in time, decreases in amplitude, and prolongation of the wavelength in the gravitational waveform.

the effect observed in this work is indeed resulted from the third BH.

III. NUMERICAL RESULTS

There is an obvious hierarchical structure in the considered system, as shown in Fig. 1. A small BBH system and a third BH, which is distant and much more massive, form a bigger binary system. From the point view of eccentricity e of a binary, there are two limits of the possible configurations existing in the universe : a head-on collision ($e = 1$) and (quasi-)circular orbit ($e = 0$). Here we would like to investigate four possible combinations of the limiting cases in order to offer some clues for understanding this kind of astrophysical system.

The considered hierarchical structure comprises four possible cases. They are (A) the head-on-freefall case: a BBH is in the process of a head-on collision while its center of mass (CoM) freefalls toward a third BH; (B) the head-on-orbiting case: a BBH is in the process of a head-on collision while its CoM circularly orbits a third BH; (C) the inspiral-freefall case: a BBH is in the process of a quasi-circular inspiral while its CoM freefalls toward a third BH; (D) the inspiral-orbiting case: a BBH is in the process of a quasi-circular inspiral while its CoM circularly orbits around a third BH. The numerical results of the four scenarios will be presented in the following subsections. The total mass of the BBH in these cases is set to be $M = 1$.

We use the similar grid setup as in our previous work [57]. There are five levels of grid for the fixed mesh refinement. The physical boundary is put at $64M$. The domain takes a cubic shape, and the length of the domain in each level shrinks to one half of the length of the preceding level. For the finest level, the domain contains two boxes: they are bounded by $(-2 < x < 2, -2 < y < 2, 0.25 < z < 4.25)$ and $(-2 < x < 2, -2 < y < 2, -4.25 < z < -0.25)$, and are movable with the moving-box technique. Before the study on the effect of a third BH, the convergence of our code for an isolated BBH in a head-on collision is tested. The fourth order convergence of Ψ_4 is shown in Fig. 3 with the convergence factor

$$C_4 = \frac{(h_1/h_2)^4 - 1}{1 - (h_3/h_2)^4} \approx 0.65, \tag{12}$$

where $h_1 = 1/32$, $h_2 = 1/28$ and $h_3 = 1/24$ are the finest grid widths for the high, median and low resolution, respectively. Some minor disagreement for $t > 80$ was expected to come from the outer boundary which could give a second-order error.

In the study of the BBH's evolution under a gravitational background, we use the Newman-Penrose scalar Ψ_4 instead of the gravitational strain $h^{+/\times}$ to represent the gravitational wave. Ψ_4 is widely used in numerical relativity community as a measurement of gravitational waveform. So it is convenient to use Ψ_4 and its spherically harmonic decompositions, instead of $h^{+/\times}$, for comparison with previous works. Furthermore, Ψ_4 can be linked to $h^{+/\times}$ straightforwardly as explained in [4, 76].

A. Head-on-freefall case

We will consider, in this and the next subsections, the BBHs in head-on collisions while their CoMs either freefall toward or circularly orbit around the third massive

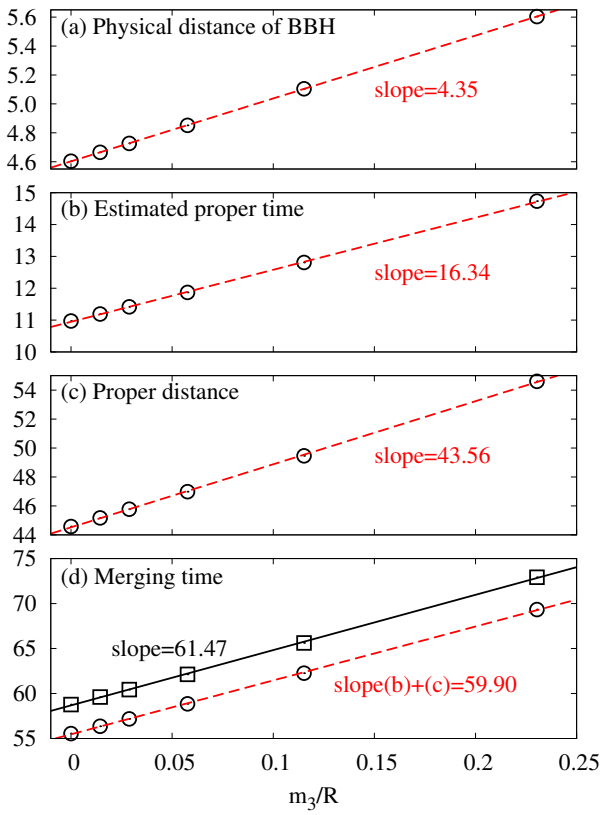

FIG. 5: (a)Initial physical distance between the small BBH, (b)proper merging time from the initial physical distance as estimated with Eq. (13), and (c)proper distance from the center of the small BBH system to the detector, respectively, with respect to the strength of the gravitational potential of the third BH. (d) Comparison of the proper merging time, which are either measured at the detector(squares) or as the direct addition(circles) of (b) the (c). The circles and squares indicate the numerical data. The slopes of their linear fitting are also given.

BH. The massive BH has the mass m_3 and is located at $(-R, 0, 0)$. We will vary the mass m_3 while fix the coordinate distance at $R = 1000$, and the ratio m_3/R will represent the strength of different gravitational potential due to the third massive BH [77].

In Fig. 4, we compare the gravitational waves from the head-on collision BBH affected by a third BH and from an isolated binary in our earlier result [57]. The BBH in both scenarios has the mass parameters $m_1 = m_2 = 0.5$ and is initially located at $(0, 0, \pm 1.1515)$, which are about the ISCO. We can see from this figure that the gravitational potential of the third BH causes a time delay, a slight decrease of the amplitude of the $\ell = 2$ mode of Ψ_4 and a prolongation of the wavelength in the waveform. We also observe at the same time the excitation of higher order modes with $\ell > 2$. The decrease in the amplitude mainly comes from the gravitational redshift caused by the third BH. Similar to the nonlinear redshift effects of an electromagnetic wave in a medium, the potential of the third BH broadens the spectrum of the gravitational wave instead of simple linear spectral redshift.

The time delay comes from three factors: (i) the delayed merger; (ii) the prolonged proper distance from the source to the detector and (iii) the change in the coordinate time. It can be understood that the last one is simply caused by the change of time gauge due to the existence of the third BH, therefore we only discuss the first two factors in detail.

Factor (i) comes from the effectively larger proper separation, i.e., the physical distance d of the BBH, due to the curved spacetime background of the third BH. Here the physical distance d is defined as the proper length of the shortest line connecting two individual apparent horizons, which is along the z-axis in the current case, and is explicitly calculable at the initial slice with $d = \int \sqrt{\gamma_{ij} \mathrm{d}x^i \mathrm{d}x^j}$ provided these two apparent horizons are found. We plot d in first panel of Fig. 5 with respect to the potential strength of the third BH. Unlike the coordinate merging time of the BBH that can be obtained from the simulation, it is ambiguous to evaluate the proper merging time because of the singularities in the BBH. Due to our perturbational treatment of the third BH's gravitational effect and the small velocity (compared with speed of light) of each BH in the head-on BBH, Newtonian mechanics can provide a rough estimate of the proper merging time for a given d by virtue of the ordinary equation,

$$\frac{\mathrm{d}^2}{\mathrm{d}t^2}\frac{\vec{d}}{2} = -m\frac{\vec{d}}{d^3} - m_3\frac{\vec{\mathcal{D}} + \vec{d}/2}{|\vec{\mathcal{D}} + \vec{d}/2|^3} \approx -m\frac{\vec{d}}{d^3}, \qquad (13)$$

where m is the mass of individual BH in the BBH, and the physical distance between the small binary and the third BH is $\mathcal{D}$. In the last term of the above equation, $\mathcal{D}$ does not appear in the final expression. However, the third BH's gravity still affects the physical distance d through its effect on the 3-metric. We integrate the above equation to obtain the estimated proper merging time for certain d, and show the results in Fig. 5b. For the factor (ii), the proper distance between the BBH system and the detector is prolonged due to the potential of the third BH. In Fig. 5c, the prolonged proper distance from the BBH to the detector was plotted with respect to the potential strength of the third BH. The prolonged proper distance should be equal to the proper time as the gravitational wave propagates in the speed of light. The two effects responsible for the proper time delay, one in the merger of head-on collision and the other in the propagation of the gravitational wave, can account for the numerically detected time delay for the gravitational wave. To verify this point, we measure the proper time of the highest peak of the gravitational wave arriving the detector(squares in Fig. 5d), and compare it with the result from the direct addition of the estimated proper merging time and the proper propagation time(circles in Fig. 5d) as mentioned. After a linear fit to get the slope as the time delay rates with respect to the extra potential, it turns out that the measured proper time delay

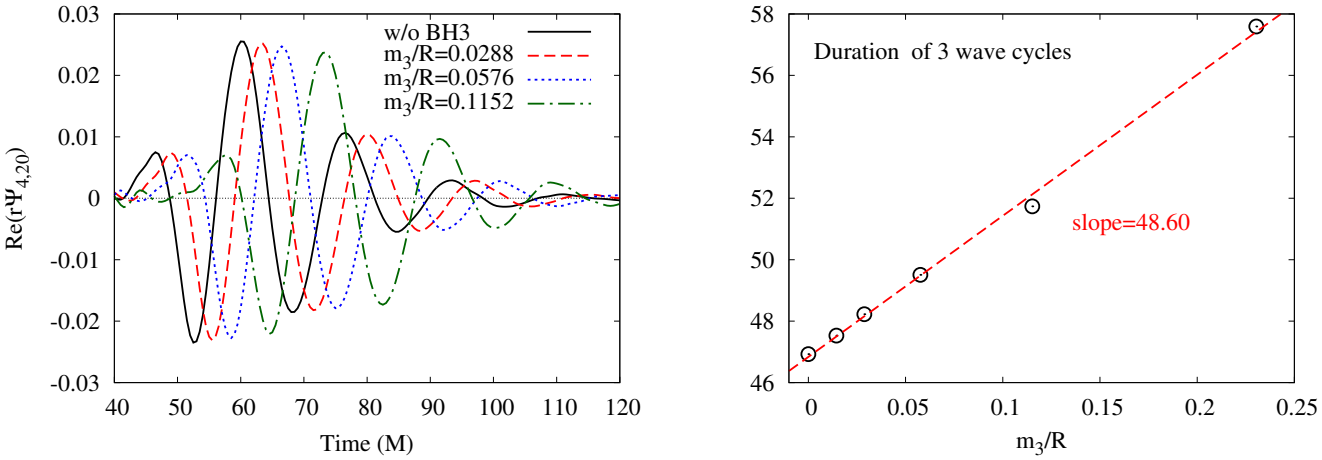

FIG. 6: Left panel: Waveforms of the head-on-freefall case in Sec. III A for different potential strengths of the third BH. The amplitude decreases as the third BH's gravitational potential increases. Right panel: duration for three wavelengths starting from the wave peak at around $t = 45$ to the peak at around $t = 90$. The wavelength increases as the third BH's gravitational potential increases.

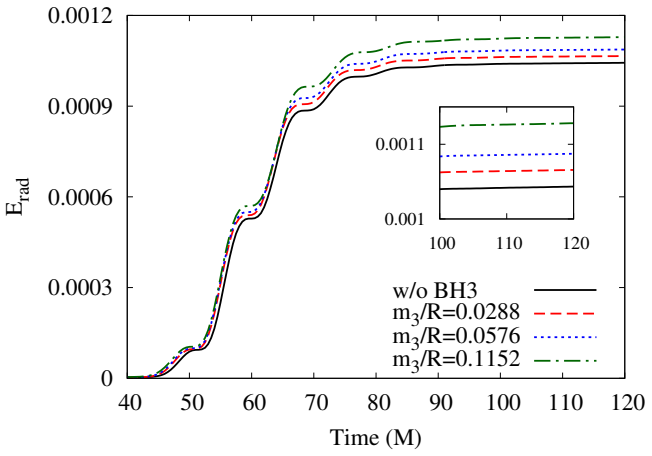

FIG. 7: Accumulated radiated energy with respect to time for different gravitational potential strengths. A stronger gravitational potential results in more energy radiation.

rate, 61.47 is very close to the sum of the delay rate of the estimated proper merging time and the proper propagation time, as shown in the Fig. 5d [78].

As mentioned earlier, the redshift effect due to the gravitational potential of the third BH will decrease the amplitude of Ψ_4's $\ell = 2$ mode as well as prolonging the wavelength of the gravitational waveform. They are clearly shown in Fig. 6, where the stronger gravitational potential causes smaller amplitude as in the left panel, and the longer durations of three cycles (from the first to the third peak in the left panel), i.e., the longer wavelength as shown in the right panel.

We also investigate the gravitational energy radiation for this case and show the result in Fig. 7. It shows that a stronger gravitational potential results in more energy radiation. This can be understood as follows: when the small BBH system is located in the gravitational potential of a third BH, the potential energy will be put into the binary system due to the interaction, and some part of this energy is carried out by the gravitational wave. Then the radiation energy during the head-on collision is enhanced by the potential of the third BH. Campanelli *et al.* [50] have studied the ISCO problem for triple BH systems. They concluded that the third BH will enhance the gravitational radiation of BBH, which is consistent with our numerical result. In our perturbational treatment, the curved background is fixed and thus there is no back-reaction between the BBH and the third BH. In a more realistic case, the back-reaction will speed up the free-falling process of the BBH toward the third BH.

Besides distorting the $\ell = 2$ modes, the existence of the third BH also induces higher-order modes, especially the $\ell = 3$ modes, in the BBH's gravitational radiation. The left panel of Fig. 8 shows the waveform of the ($\ell = 3$, $m = 1$) mode of the gravitational radiation induced in the current case with respect to the different strength of the gravitational potential. The right panel of Fig. 8 shows the amplitudes of the ($\ell = 3$, $m = 1$) mode of the gravitational wave, which demonstrates a nonlinear growth with respect to the strength of the third BH's gravitational potential. In principle, it is possible for the nonlinear growth of the $\ell = 3$ mode to be used as a signature to distinguish a three-BH system from a BBH system. However, the phenomenon could also complicate the identification of the source of the gravitational wave. Even in the Newtonian framework, certain three-body system with the same quadrupole wave forms may have quite distinguishable higher-order modes of the gravitational wave [55]. Without a careful understanding on the waveform pattern, the gravitational wave emitted from a three-BH system, like the cases described in this work, could be misidentified as one from an unequal-mass BBH

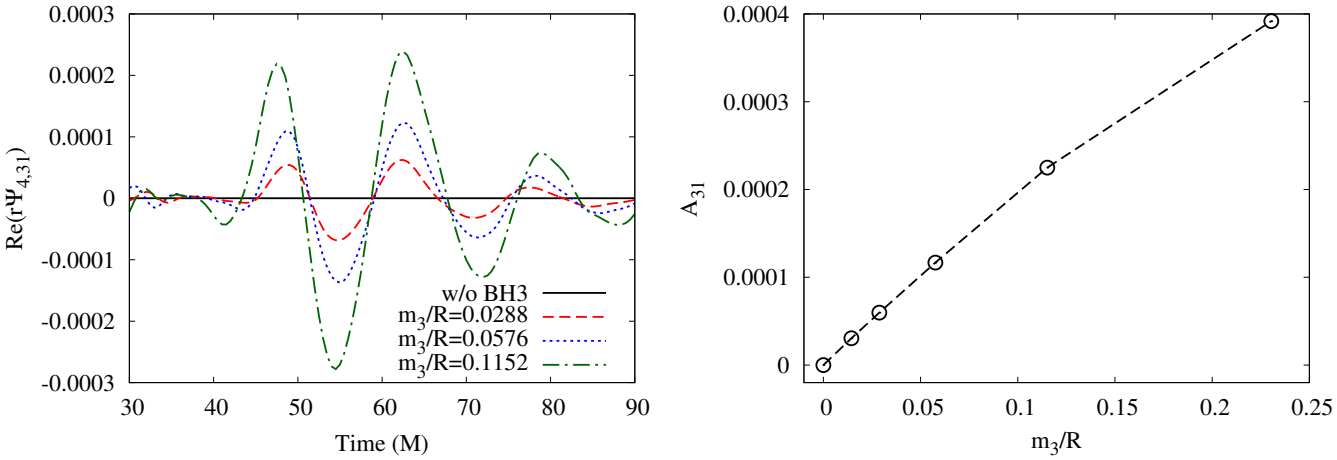

FIG. 8: Left panel: Waveforms of the ($\ell = 3$, $m = 1$) mode of Ψ_4 for different background potential strengths. Right panel: The largest amplitude of $\Psi_{4,31}$ showing a nonlinear growth pattern.

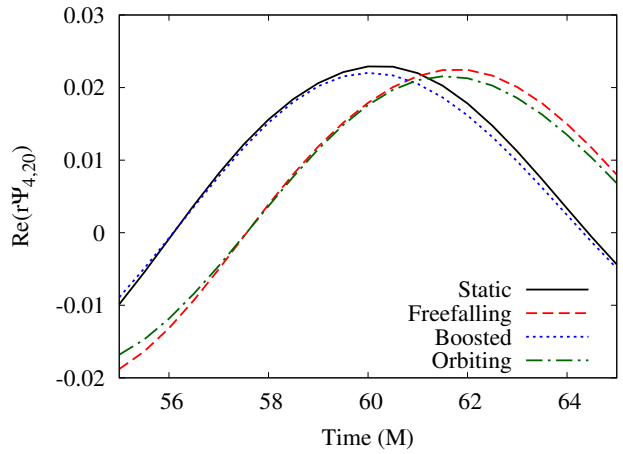

FIG. 9: Waveforms of $\mathrm{Re}(r\Psi_{4,20})$ for four scenarios mentioned in Sec. III B. These results show that the relativistic Doppler effect on the behavior of the gravitational waveform is much less important than the gravitational redshift effect in the head-on-orbiting case.

system in which the higher-order modes of gravitational wave also exist.

B. Head-on-orbiting case

In this subsection, we study the head-on collision of a BBH while the BBH system moves along a circular orbit around a third large BH. The orbiting velocity of the center of mass (CoM) of the BBH is initially set according to the Newtonian gravity, i.e., $v^2 \approx m_3/R$. This treatment is valid since the third massive BH is distant to the BBH and the orbit of the BBH is set to be circular. In fact, the massive BH are so distant such that by the end of merger of the BBH, the CoM displacement of BBH is only a little fraction of one big orbit, which makes the eccentricity of the big orbit not relevant to our study. Given the linear momentum parameters and the position parameters of the BHs, we solve the puncture initial data as described in Sec. II B. For the third large BH, we fix the coordinate distance at $R = 1000$ as in the previous subsection, and change the gravitational potential m_3/R by varying the mass parameter m_3.

There are two effects for a BBH orbiting in the gravitational potential well of a third large BH: the relativistic Doppler effect and the gravitational redshift. In order to identify the importance of these two effects on the time delay in the gravitational waveform in the current case, we compare the waveforms obtained from the following four scenarios: (i) the head-on collision of an isolated BBH; (ii) the head-on collision of a BBH freefalling towards a third large BH; (iii) the head-on collision of a boosted isolated BBH; (iv) the head-on collision of a BBH orbiting around a third large BH. Here the mass parameter of the third BH is set to be $m_3 = 14.4$, the same in the cases of (ii) and (iv), and the boosting velocity in (iii) is set to be the same as the orbiting velocity in (iv), the magnitude of which is 0.12, according to $v^2 \approx m_3/R$ and $R = 1000$. The results in Fig. 9 show that the waveforms of cases (i) and (iii) are close to each other. So are the waveforms of cases (ii) and (iv). This indicates that the gravitational redshift of the third large BH should dominate the effect on the time delay of the gravitational wave in the merging process of a BBH. On the contrary, the relativistic Doppler effect has only minor influence on the time delay of the waveform. Therefore we will neglect in the following discussion the relativistic Doppler effect due to the small orbiting velocity of the CoM of a BBH around a third large BH, and focus mainly on its gravitational redshift effect.

In order to let the BBH move slow enough such that it will stay inside the computational domain during the merger process, and thus we can keep the necessary ac-

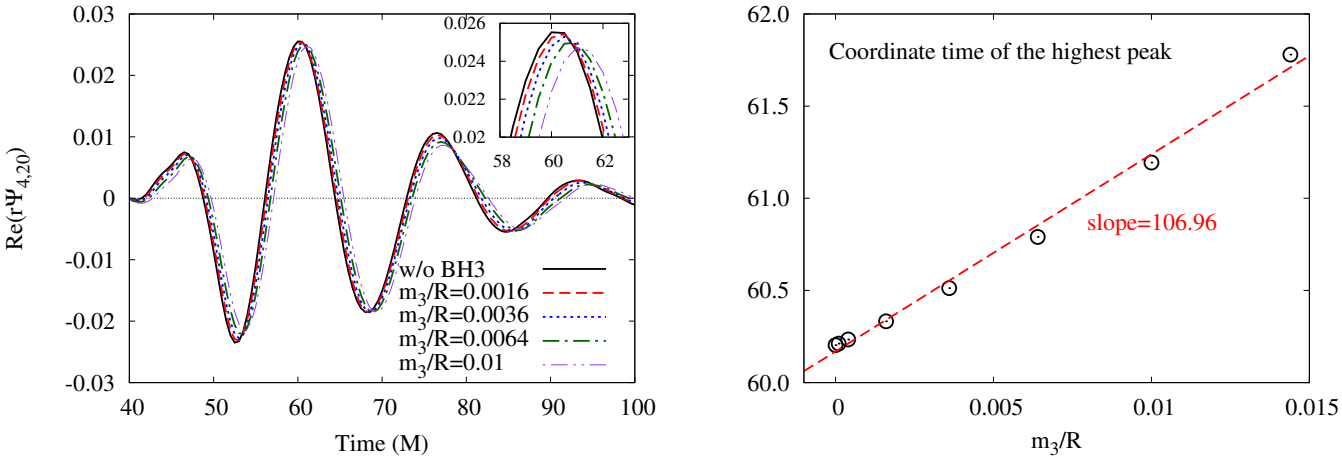

FIG. 10: Left panel: Waveforms of the head-on-orbiting case in Sec. III B for different background potential strengths. They are qualitatively similar to Fig. 6, except the smaller decreasing amplitude due to the smaller background potential strength. Right panel: coordinate time of the highest peak of $\Psi_{4,20}$ arriving the detector for different background potential strengths.

curacy during the generation of gravitational wave, the gravitational potential strength of the third BH is set to be smaller than in the previous subsection. The numerical results for this case show that all phenomena including the time delay of the waveform, the decrease of the wave amplitude, the prolongation of the wavelength, the enhancement of the energy radiated, and the excitation of the higher-order modes are qualitatively similar to the ones in the previous case. Therefore we only show here the decrease in amplitude of the gravitational waveform and the coordinate time delay of the highest peak of $\Psi_{4,20}$ with respect to different potential strengths in Fig. 10. It can be seen in the left panel that the decrease in amplitude of the waveform is less than that obtained in the previous subsection due to the smaller gravitational potential strength of the third BH. Just as in the previous subsection, the orientation of the small BBH barely affects the result in this case because of the negligible tidal effect from the third BH in a head-on collision.

C. Inspiraling-freefall case

In this and the next subsections, we will consider the effect of a third massive BH on an inspiraling BBH. The two BHs of the BBH initially have the the irreducible masses $m_1 = m_2 \approx 0.5$ and are located at $(0, 0, \pm\frac{D}{2})$. The third BH has mass $m_3 = 5 \times 10^4$ and is located at $(R, 0, 0)$.

In this subsection, we study the inspiral-to-merger evolution of a BBH while the CoM of the BBH freely falls towards the third large BH. The left panel of Fig. 11 shows the evolution of a typical inspiraling trajectory of the BBH, from the initial coordinate separation $D = 4.5$, affected by the third large BH located at $(R = 5\times10^6, 0, 0)$. We can see from the plot that the gravitational potential of the third large BH leads to an increase in the eccentricity of the trajectory of the BBH, compared with that of an isolated BBH. The right panel of Fig. 11 shows a typical comparison of the gravitational waveforms for the BBH inspiraling with and without the influence of a third large BH. It can be seen that the gravitational potential of the third large BH causes a time advance, a prolongation of the wavelength, and a somehow complicated variation in the amplitude of the gravitational waveform.

As explained in Sec. III A, the time delay for the existence of a third large BH in a head-on collision arises from three factors: the delayed merger process, the prolonged proper distance, and the change of the coordinate time. For an inspiraling process of a BBH, there exists another effect, i.e., a change of the eccentricity, as shown in the left panel of Fig. 11. It is obvious that the change of the eccentricity is mainly caused by the tidal effect of the third large BH. As a BBH system emits more gravitational radiation in an elliptical orbit than in a circular orbit [79, 80], the increase of eccentricity is expected to expedite the merger process of the BBH. Therefore, the time shift in the inspiraling process is the result of competition between the increase in eccentricity and the others. Here we look at this in more detail.

From the right panel of Fig. 11 we can see that the waveform is affected by both the time delay and time advance phenomena: the spurious radiation part of the waveform is delayed, while the burst part is advanced. The beginning of the waveform, near $t = 50$, is a result of the spurious radiation hidden in the initial data. Thus, this part is independent of the merging process of a BBH. Here we can see a time delay because of the prolonged proper distance from the BBH to the detector, at $r = 40$, due to the existence of the third BH. In the main part of the merging process, starting at the coordinate time $t \approx 100$, we can clearly see the time advance effect. This is due to the increase in eccentricity under the influence

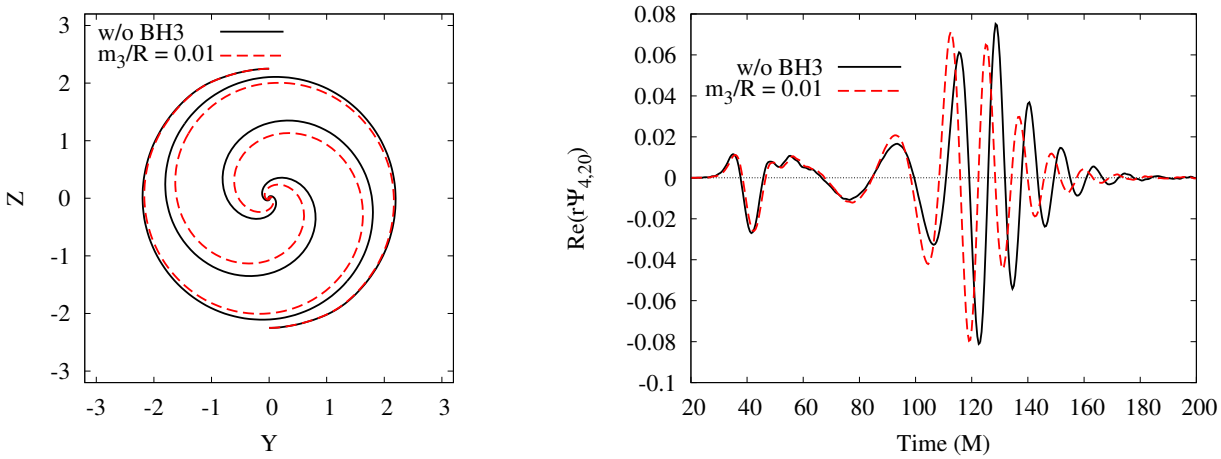

FIG. 11: Left panel: Typical inspiral trajectories for an isolated inspiraling BBH and for the inspiraling-freefall case in Sec. III C. The solid curve indicates the trajectory of an isolated BBH and shows a quasi-circular inspiral shape. The (red) dashed curve indicates the trajectory of the BBH in the gravitational potential well of the third BH with $m_3 = 5 \times 10^4$ which is located at $(R = 5 \times 10^6, 0, 0)$. There is a change in the eccentricity of the (red) dashed curved when compared with the solid line. Right panel: Real components of $r\Psi_{4,20}$ for an isolated inspiraling BBH and for the inspiraling-freefall case. The red dashed (black solid) line indicates the case with (without) the third BH. The detector is located at $r = 40$. It can be seen that the gravitational potential of the third BH causes a tiny time delay in the spurious part and the effect of a time advance in the major part of the waveform.

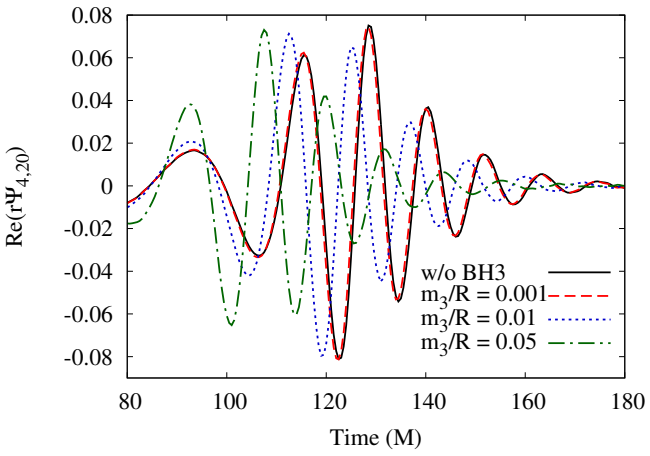

FIG. 12: The Re$[r\Psi_{4,20}]$ for the inspiraling-freefall case for different potential strengths of the third BH. The results show the effect of advance in time and the prolongation of the wavelength in the burst part due to the third BH's gravitational potential. The effect of advance in time is obvious and much larger than in the spurious radiation (refer to Fig. 11). The amplitude first increases and then decreases in the wave-train. And the variation becomes bigger as the gravitational potential of the third BH becomes larger. This detail is explained in the context.

of the gravitational potential of the third large BH. Obviously the effect of the eccentricity increase overtakes other time delay factors in the competition.

Besides the effect of time advance, there is another feature shown in the waveform. If we take the highest peak in the wave-train of Ψ_4 roughly as the time of merger [4], this divides the waveform in the gravitational wave-train into two kinds of different behaviors: Before the merger, the wave amplitude of Ψ_4 becomes larger as the gravitational potential of the third large BH becomes larger. This is because the increase in eccentricity of the BBH's trajectory is the dominant effect in speeding up the inspiral-to-merger process compared to the isolated case. This results in stronger gravitational radiation. After the merger, the wave amplitude of Ψ_4 turns out to become smaller as the gravitational potential of the third BH becomes larger. The decrease in the amplitude of the gravitational waveform mainly arises from the stronger redshift effect due to the existence of the third BH. These phenomena are illustrated in the right panels of Fig. 11 and in Fig. 12.

In fact, the inspiral-freefall case has been studied in [50] as an initial data problem. Based on the result of its ISCO initial data, it was conjectured in the work that the third BH will (1) increase the terminal amplitude of the inspiral gravitational waveform; (2) increase the duration of the pre-plunge phase; and (3) redshift the frequency of the gravitational wave during the pre-plunge phase. Points (1) and (3) are consistent with our current results, that the radiation power is amplified by the third BH before the merging process, and that there is a gravitational redshift effect. However, point (2) seems to conflict with our time-advance result. Therefore, we need to look deeper into this point. After a thorough study, we discover that as the initial separation of BBH increases, the phase change of the gravitational wave (due to the effect of the third large BH) transits from a time-delay to a time-advance, as shown in Fig. 13. Note that the ISCO separation case studied in [50] corresponds to the

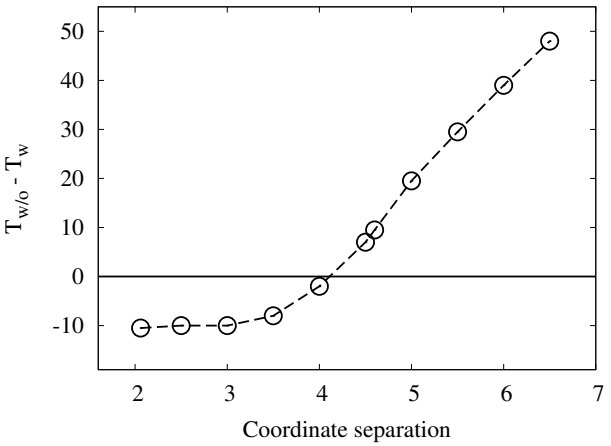

FIG. 13: Time difference of the inspiral-to-merger process between an isolated BBH and the inspiral-freefall case in Sec. III C. Here the merging time is the coordinate time corresponding to the maximal amplitude of the $\Psi_{4,20}$ waveform. The time difference ranges from being negative, i.e., time-delay, to being positive, i.e., time-advance, as the initial separation increases. In this case the turning point is around $r \approx 4.2$.

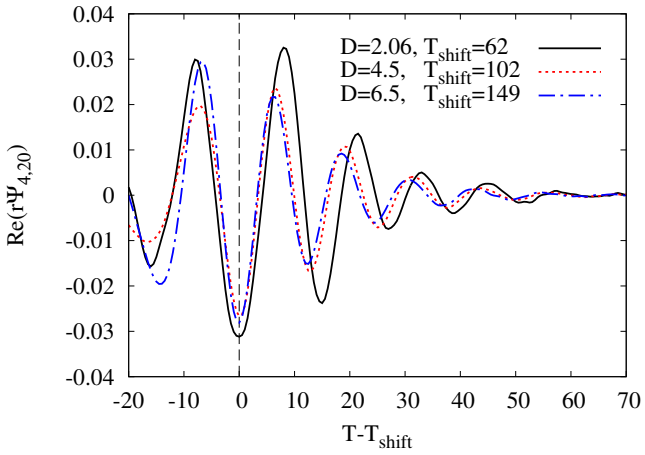

FIG. 14: Time-shifted waveforms of $r\Psi_{4,20}$ in the inspiral-to-merger process of a BBH, with different initial separations, under the influence of a third BH in the inspiral-freefall case. $T - T_{\rm shift} = 0$ is the shifted merging time defined at the maximal amplitude, and these waveforms do not match with each other despite of the shifting.

leftest data point in this figure, which is time-delay. One possible explanation for the result is that, since the initial separation is small, the gravitational redshift effect caused by the existence of a third large BH is dominant in the evolution of the BBH and the merging time is delayed. On the other hand, the eccentricity effect by a third large BH outweighs the gravitational redshift effect when the initial separation of the BBH becomes large enough, and thus the merging time is advanced. In other words, the time difference in the inspiral-to-merger process of a BBH under the influence of a third large BH is dependent on the initial separation.

In Fig. 13, We do not expect the time difference to converge when the separation range is still very short, compared with a fixed R (the distance to the third BH). Since the tidal effect on the evolution of the BBH due to the existence of the third large BH is accumulative during the BBH's inspiral, we could expect that the time-difference will keep increasing as the initial separation of the BBH becomes larger [81]. It is known that the gravitational waveform from the merger of a BBH with the ISCO as the initial separation should agree with the waveforms just before the merger from different initial separations. However, this understanding is based on the assumption that the BBH is isolated. It is not the case when there exists an external gravitational potential background. The final result should come from the competition between the circularization effect from the gravitational radiation and the tidal effect from the external gravitational potential background. It seems not exist related investigations on this issue in the literature. Therefore, we turn to check our numerical result. In Fig. 14, it shows that the gravitational waveforms from different initial separations between the two BHs in a BBH system under an external gravitational potential do not match with one another even the merging times have been shifted to be the same. From our numerical experiments, it shows that the gravitational circularization effect could not relax totally the accumulated eccentricity from the tidal effect caused by the external gravitational potential background. A detailed investigation is needed to have a better understanding on this phenomenon in the future.

Compared with the head-on collision of a BBH as discussed in Sec. III A, the higher-order mode effect due to the existence of a third BH in the inspiraling process is more evident. The left panel of Fig. 15 shows the amplitude of $\mathrm{Re}(r\Psi_{4,33})$ produced during the inspiral-to-merger process of a BBH with respect to different potential strengths of a third BH. The higher-order mode, $\mathrm{Re}(r\Psi_{4,33})$, shows a nonlinear dependence on the strength of the gravitational potential, as shown in the right panel of Fig. 15. This result is consistent with those detailed in the previous two subsections: This nonlinear phenomenon could be a signature distinguishing a three-BH system from a BBH system, as well as complicating the identification of the source of a gravitational wave.

D. Inspiraling-orbiting case

In this subsection, we investigate the inspiral-to-merger process of a BBH orbiting around a third large BH. Initially, the CoM of the BBH moves around the third large BH in a circular orbit. Therefore, the velocity of the CoM of the BBH can be approximated by Newtonian mechanics. Similar to the previous subsection, the two small BHs with the irreducible mass $m_1 = m_2 \approx 0.5$ are located at $(0, 0, \pm\frac{D}{2})$ initially. We put the third BH

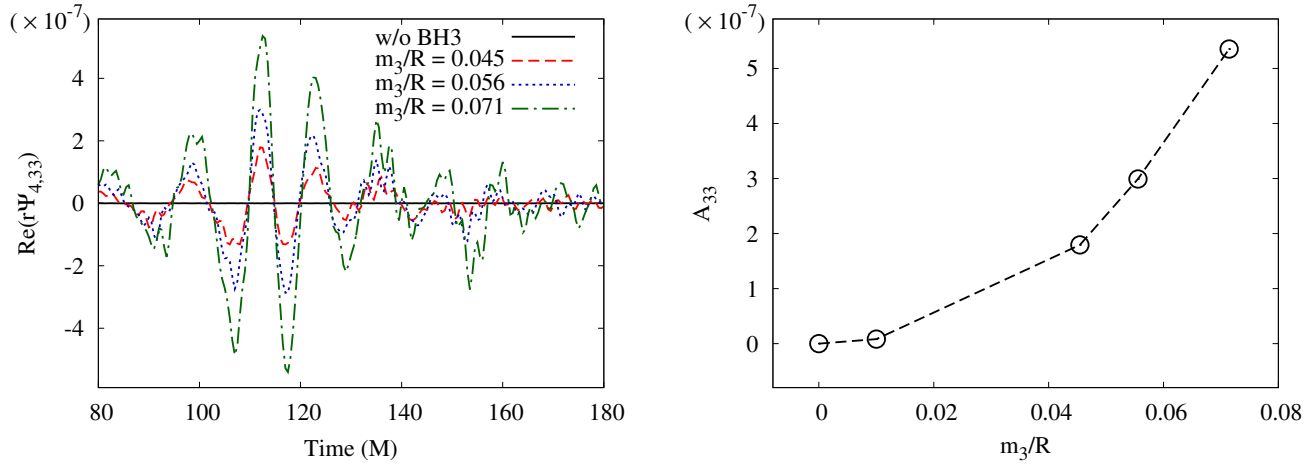

FIG. 15: Left panel: Comparison of $\mathrm{Re}(r\Psi_{4,33})$ in the inspiraling-freefall case with respect to different potential strengths of a third large BH. The existence of the third BH induces the higher-order ($\ell = 3$) mode and quite a large amount of the radiation is emitted away in this mode. Right panel: Highest peaks of $\mathrm{Re}(r\Psi_{4,33})$ with respect to different potential strengths of the third BH. The nonlinear behavior of the higher-order ($\ell = 3$) mode with respect to the gravitational potential strength of the third BH is shown.

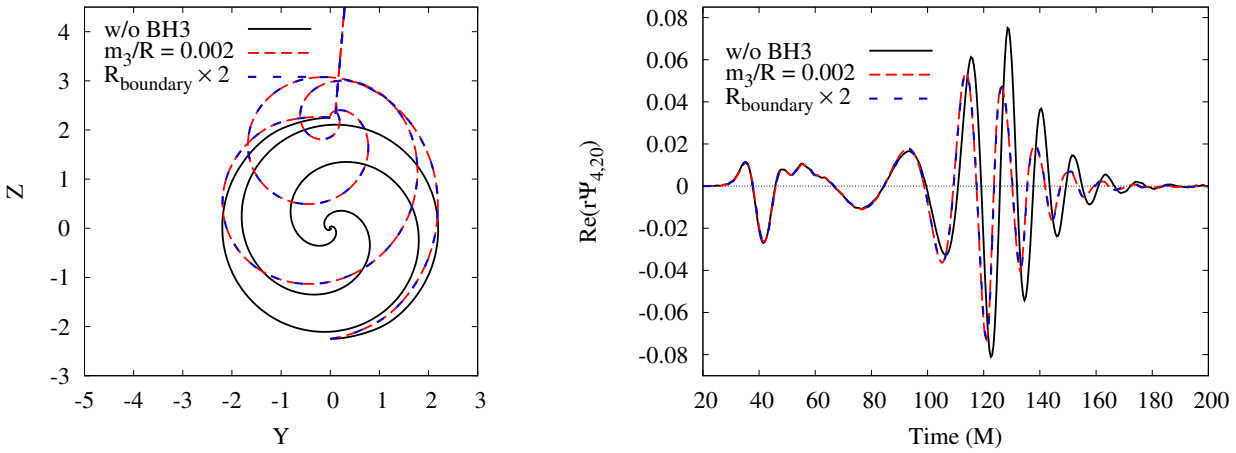

FIG. 16: Left panel: Typical trajectories for an isolated inspiraling BBH and the inspiraling-orbiting case in Sec. III D. The solid quasi-circular inspiral curve is for an isolated BBH. The red dashed curve indicates the trajectory under the gravitational potential of the third BH with $m_3 = 5 \times 10^4$ at $(R = 2.5 \times 10^7, 0, 0)$. The blue long-dashed line represents the same case but with a doubled outer boundary. Right panel: The corresponding waveforms of $r\Psi_{4,20}$. The red-dashed (black-solid) line indicates the case with (without) the third BH. The blue long-dashed line represents the case same as the one for the red dashed curve but with a doubled outer boundary. It can be seen that, besides the decrease in the wave amplitude, the gravitational potential of the third BH causes a tiny time delay in the spurious part and a time advance in the major part of the waveform.

at $(R, 0, 0)$. In order to get a circular orbit for the BBH around the third large BH, we use the quantity $\sqrt{m_3/R}$ to evaluate the velocity of the CoM of the BBH with respect to the third BH. This velocity is then vectorially added to the quasi-circular orbiting velocity of each BH of the BBH. We have ever tried measuring the eccentricity of the small BBH affected by the background to check if any extra eccentricity is introduced by the vectorial addition. It turns out that there is no observable extra eccentricity introduced by this addition during the whole inspiral stage. For the third large BH, we fix its mass parameter $m_3 = 5 \times 10^4$ as in the previous subsection while varying its coordinate distance R. Given the mass parameters, the linear momenta and the positions of the *three* BHs, the puncture initial data was constructed as described in Sec. II B.

The left panel of Fig. 16 shows a typical trajectory of the BBH with the initial coordinate separation $D = 4.5$ for the current case, where the third large BH is located at $(R = 2.5 \times 10^7, 0, 0)$. It can be understood from the plot that the CoM of the BBH moves roughly along a Newtonian circular orbit around the third large BH. The trajectory is in fact the combination of the orbit of the CoM of the BBH and the BBH's inspiraling around the

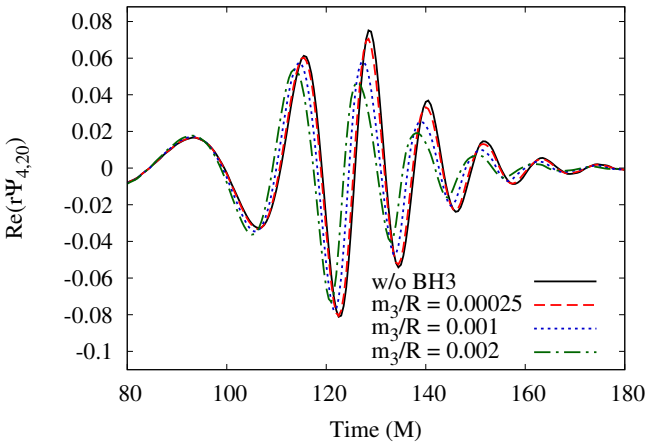

FIG. 17: The $\mathrm{Re}(r\Psi_{4,20})$ in the inspiraling-orbiting case with respect to different potential strengths of the third BH. Due to the existence of the third BH, the time advance effect is clear and different from the spurious radiation part, and the one for the inspiraling-freefall case (compare Fig. 12). The amplitude decreases as the gravitational potential of the third BH becomes stronger.

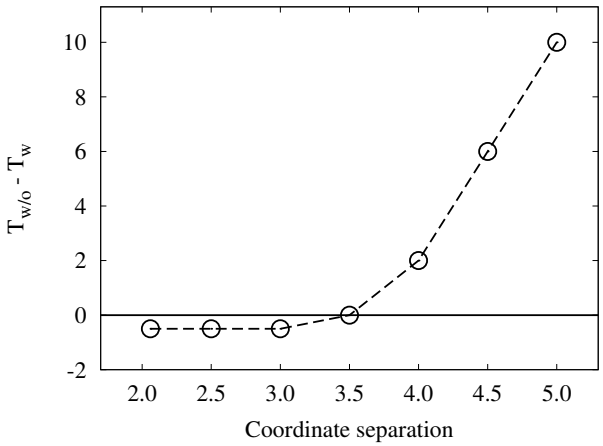

FIG. 18: Time difference of the inspiral-to-merger process between an isolated BBH and the inspiraling-orbiting case in Sec. III D with respect to the initial separation. Here the merging time is the coordinate time corresponding to the maximal amplitude of the $\Psi_{4,20}$ waveform. The time difference ranges from being negative, i.e., time-delay, to being positive, i.e., time advance, as the initial separation increases. In this case, the turning point is around $r \approx 3.5$.

CoM, and it is quite deformed compared with the trajectory for an isolated BBH.

The gravitational waveform of the BBH in the current case is presented in the right panel of Fig. 16. Compared with the right panel of Fig. 12, we find that the effect of the third large BH on the waveform is stronger in the current case than in the inspiraling-freefall cases. In the plot, the waveform is delayed in the spurious part but advanced in the major part, caused by the gravitational potential of the third large BH. This is similar to the previous inspiraling-freefall case. In Fig. 16, we also plot the trajectory and Ψ_4 for the same scenario but with a doubled outer boundary. The perfect coincidence of them indicates that the boundary condition described in Sec. II C is reliable.

In Fig. 17, the time advance of $\mathrm{Re}(r\Psi_{4,20})$ due to the third large BH is clear and different from its spurious radiation part. This phenomenon is similar to the one in the inspiraling-freefall case (compared with Fig. 12). Stronger gravitational potential of the third BH results in the smaller amplitude of the waveform.

The shift of the waveform due to the gravitational background of the third BH are quantitatively shown in Fig. 18, in which it indicates the transition from the time-delay to time-advance as the initial separation of BBH increases. Similar to the previous case, the possible explanation for the change in the time difference of the inspiral-to-merger process of a BBH under the influence of a third large BH compared with the one of an isolated BBH, arises from the competition between the eccentricity effect and the gravitational redshift effect. Compared with the previous (inspiraling-freefall) case in which the $(\ell = m = 3)$ mode of Ψ_4 is dominant among the higher modes, the $(\ell = 3, m = 0)$ modes of Ψ_4 is dominant in the current case, as shown in the left panel of Fig. 19. The orbiting of the BBH along the x-z plane accounts for this effect. In addition, the amplitude of the $(\ell = 3, m = 0)$ mode of $\mathrm{Re}(\Psi_4)$ increases nonlinearly.

IV. SUMMARY AND DISCUSSION

Motivated by the fact that most BBH systems are located in the gravitational potential of a super-massive BH hosted in the center of a galaxy, we investigate the effect of the potential on the dynamics of a BBH system. Instead of the heavily numerical calculation of the evolution of the three-BH problem with a fully relativistic treatment, we use a perturbational scheme to investigate the effect of the gravitational potential from a third large BH on the evolution of a BBH, especially on the waveform of gravitational radiation. In our perturbation method, we ignore the back-reaction of the BBH system on the third large BH, regarding the third BH as a background for the BBH system.

The scenarios we consider include the head-on collision and the inspiral-to-merger process of a BBH in the cases of the BBH system freefalling towards, or circularly orbiting around the third large BH, which are considered as the two limits in all possible configurations. The effect of the gravitational potential from a third BH on a BBH system in our study includes: (1) the gravitational redshift effect, including the prolongation of proper distance, the prolongation of the wavelength, the decrease of the waveform amplitude; (2) the increase in the eccentricity which is from the tidal effect of the third large BH and expedites the merger of a BBH system; (3) delaying

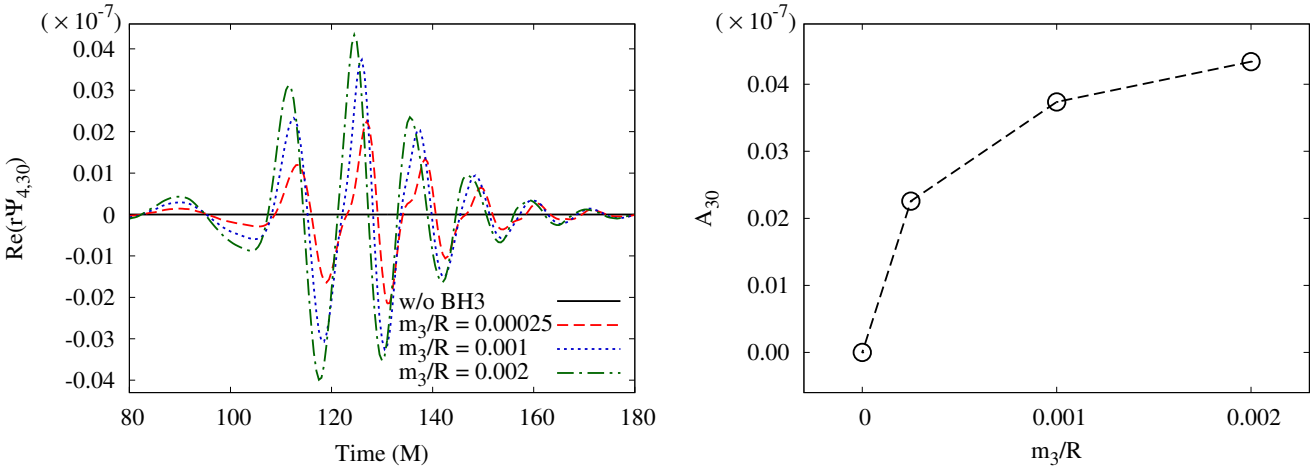

FIG. 19: Left panel: Comparison of $\mathrm{Re}(r\Psi_{4,30})$ in the inspiraling-orbiting case for different potential strengths of a third BH (cf. Fig. 15). The amplitude is much larger than that in the inspiraling-freefall case. Right panel: Highest peak with respect to different potential strengths of the third BH. The nonlinear behavior of the $\ell = 3$ mode and the behavior of the curve are different from the one in the inspiraling-freefall case.

or advancing the merging process of the BBH, which depends on the competition between the gravitational redshift effect and the eccentricity effect; (4) inducing the higher-order modes in the gravitational waveform. The orientation of the BBH system hardly affects the above results. It is interesting that (4) supports the conjecture proposed in [55] in the full GR regime. This might provide valuable information for gravitational wave astronomy to distinguish whether the detected BBH system is isolated or located in the potential of a super-massive BH.

In this work, for the $\ell < 3$ modes, all the quantities are linearly dependent on the gravitational potential m_3/R, which validates the usage of the perturbation method. In most realistic cases, the gravitational potential is much weaker than the cases considered in this work. Therefore the perturbation method is expected to be applicable to most realistic cases.

The third BH in our case introduces a non-axisymmetric background feature, which makes the issue of gravitational wave extraction even more complicated. However, considering the detector located at the weak field region and finitely separated from both the merging binary and the massive BH, we adopt the usual approach to extract the information of gravitational radiation via the Newman-Penrose Scalar Ψ_4. A possible extension of the work would be a detailed study on the more rigorous way to extract the radiation under a background and the dependence of the modification on the relative position of the binary, detector and the background source.

We have considered the evolution of an equal-mass BBH under the influence of a third large BH. The study can be generalized to an unequal-mass BBH system. The major effects from the third large BH on a BBH are shown qualitatively in this study. The results indicate that these phenomena could introduce complications or even be misleading in the identification of the source of gravitational wave without further study to distinguish the signatures of a BBH in a background gravitational potential from the ones of an isolated BBH.

Acknowledgments

We thank F. Pretorius, H. Pfeiffer, E. Schnetter, and Y. Zlochower for their useful discussion. This work was supported in part by the National Science Council under the grants NSC98-2112-M-006-007-MY2 and NSC100-2112-M-006-005. Z. Cao was supported by the NSFC (No. 10731080 and No. 11005149). This work was also supported in part by the National Center of Theoretical Sciences. We are grateful to the National Center for High-performance Computing for the use of their computer time and facilities. We are also grateful to the Academia Sinica Computing Center for providing computing resource.

[1] F. Pretorius, Phys. Rev. Lett. **95**, 121101 (2005).
[2] M. Campanelli *et al.*, Phys. Rev. Lett. **96**, 111101 (2006).
[3] J.G. Baker *et al.*, Phys. Rev. Lett. **96**, 111102 (2006).
[4] A. Buonanno, G. Cook, and F. Pretorius, Phys. Rev. D **75**, 124018 (2007).
[5] J. Baker, J. van Meter, S. McWilliams, J. Centrella, and B. Kelly, Phys. Rev. Lett. **99**, 181101 (2007).
[6] M. Boyle, D. Brown, L. Kidder, A. Mroue, H. Pferffer,

M. Scheel, G. Cook, and S. Teukolsky, Phys. Rev. D **76**, 124038 (2007).
[7] B. Vaishnav, I. Hinder, F. Herrmann, and D. Shoemaker, Phys. Rev. D **76**, 084020 (2007).
[8] J. Baker, S. McWilliams, J. van Meter, J. Centrella, D. Choi, B. Kelly, and M. Koppitz, Phys. Rev. D **75**, 124024 (2007).
[9] P. Ajith *et al.*, Class. Quantum Grav. **24**, S689 (2007).
[10] A. Buonanno *et al.*, Phys. Rev. D **76**, 104049 (2007).
[11] T. Baumgarte, P. Brady, J. Creighton, L. Lehner, F. Pretorius, and R. DeVoe, Phys. Rev. D **77**, 084009 (2008).
[12] Y. Pan *et al.*, Phys. Rev. D **77**, 024014 (2008).
[13] S. Husa, M. Hannam, J. González, U. Sperhake, and B. Brügmann, Phys. Rev. D **77**, 044037 (2008).
[14] M. Hannam, S. Husa, U. Sperhake, B. Brügmann, and J. González, Phys. Rev. D **77**, 044020 (2008).
[15] B. Krishnan, C.O. Lousto, and Y. Zlochower, Phys. Rev. D **76**, 081501 (2007).
[16] J. Baker *et al.*, Astrophys. J. **653**, L93 (2006).
[17] C. Sopuerta, N. Yunes, and P. Laguna, Phys. Rev. D **74**, 124010 (2006).
[18] J. González, U. Sperhake, B. Bruegmann, M. Hannam, and S. Husa, Phys. Rev. Lett. **98**, 091101 (2007).
[19] C. Sopuerta, N. Yunes, and P. Laguna, Astrophys. J. **656**, L9 (2007).
[20] F. Herrmann, I. Hinder, D. Shoemaker, and P. Laguna, AIP Conf. Proc. **873**, 89 (2006).
[21] F. Herrmann, I. Hinder, D. Shoemaker, and P. Laguna, Class. Quantum Grav. **24**, S33 (2007).
[22] M. Campanelli, C. Lousto, Y. Zlochower, and D. Merritt, Astrophys. J. **659**, L5 (2007).
[23] M. Koppitz *et al.*, Phys. Rev. Lett. **99**, 041102 (2007).
[24] D. Choi, B. Kelly, W. Boggs, J. Baker, J. Centrella, and J. Meter, Phys. Rev. D, **76**, 104026 (2007).
[25] J. González, M. Hannam, U. Sperhake, B. Brügmann, and S. Husa, Phys. Rev. Lett. **98**, 231101 (2007).
[26] J. Baker *et al.*, Astrophys. J. **668**, 1140 (2007).
[27] M. Campanelli, C. Lousto, Y. Zlochower, and D. Merritt, Phys. Rev. Lett. **98**, 231102 (2007).
[28] E. Berti *et al.*, Phys. Rev. D **76**, 064034 (2007).
[29] W. Tichy and P. Marronetti, Phys. Rev. D **76**, 061502 (2007).
[30] F. Herrmann, I. Hinder, D. Shoemaker, P. Laguna, and R. Matzner, Phys. Rev. D **76**, 084032 (2007).
[31] M. Campanelli, C. Lousto, and Y. Zlochower, Phys. Rev. D **74**, 084023 (2006); C. Lousto, and Y. Zlochower, Phys. Rev. D **76**, 041502 (2007); M. Campanelli, C. Lousto, Y. Zlochower, B. Krishnan, and D. Merritt, Phys. Rev. D **75**, 064030 (2007).
[32] L. Boyel, M. Kesden, and S. Nissanke, Phys. Rev. Lett., **100**, 151101 (2008); L. Boyel and M. Kesden, Phys. Rev. D, **78**, 024017 (2008).
[33] W. Tichy and P. Marronetti, Phys. Rev. D **78**, 081501 (2008).
[34] P. Marronetti, W. Tichy, B. Brügmann, J. González, and U. Sperhake, Phys. Rev. D **77**, 064010 (2008).
[35] L. Rezzolla, E. Barausse,E. Dorband, D. Pollney, C. Reisswig, J. Seiler and S. Husa, Phys. Rev. D **78**, 044002 (2008); L. Rezzolla, P. Diener, E. Dorband, D. Pollney, C. Reisswig, E. Schnetter, and J. Seiler, Astrophys. J. **674**, L29 (2008); L. Rezzolla, Class. Quantum Grav. **26**, 094023 (2009).
[36] M. Washik, J. Healy, F. Herrmann, I. Hinder, D. Shoemaker, P. Laguna, and R. Matzner, Phys. Rev. Lett. **101**, 061102 (2008); J. Healy, P. Laguna, R. Matzner, and D. Shoemaker, Phys. Rev. D **81**, 081501 (2010).
[37] M. Campanelli, C.O. Lousto, and Y. Zlochower, Phys. Rev. D **77**, 101501 (2008).
[38] C.O. Lousto, and Y. Zlochower, Phys. Rev. D **77**, 024034 (2008).
[39] U. Sperhake, V. Cardoso, F. Pretorius, E. Berti, and J. González, Phys. Rev. Lett., **101**, 161101 (2008); U. Sperhake, V. Cardoso, F. Pretorius, E. Berti, T. Hinderer, and N. Yunes, Phys. Rev. Lett., **103**, 131102 (2009).
[40] B. Krishnan, C. Lousto, and Y. Zlochower, Phys. Rev. D **76**, 081501 (2007); M. Campanelli, C. Lousto, and Y. Zlochower, Phys. Rev. D **79**, 084012 (2009).
[41] J. van Meter *et al.*, arXiv:0908.0023.
[42] G. Lovelace *et al.*, Phys. Rev. D **82**, 064031 (2010).
[43] A. Abramovici *et al.*, Science **256**, 325 (1992).
[44] B. Caron *et al.*, Class. Quantum Grav. **14**, 1461 (1997).
[45] H. Lück, Class. Quantum Grav. **14**, 1471 (1997).
[46] M. Ando *et al.*, Phys. Rev. Lett. **86**, 3950 (2001).
[47] K. Danzmann *et al.*, LISA Pre-Phase-A report, 2nd ed. (1998).
[48] B. Aylott *et al.*, Class. Quantum Grav. **26**, 114008 (2009); B. Aylott *et al.*, Class. Quantum Grav. **26**, 165008 (2009).
[49] T. Damour and A. Nagar, Phys. Rev. D **76**, 064028 (2008); A. Buonanno *et al.*, Phys. Rev. D **76**, 104049 (2007); Y. Pan *et al.*, Phys. Rev. D **77**, 024014 (2008); P. Ajith *et al.*, Class. Quantum Grav. **24**, S689 (2007); P. Ajith *et al.*, Phys. Rev. D **77**, 104017 (2008).
[50] M. Campanelli, M. Dettwyler, M. Hannam, and C.O. Lousto, Phys. Rev. D **74**, 087503 (2006).
[51] C.O. Lousto and H. Nakono, Class. Quantum Grav. **25**, 195019 (2008).
[52] P. Galaviz, B. Brügmann, and Z. Cao, Phys. Rev. D **82**, 024005 (2010).
[53] M. Campanelli, C. Lousto, and Y. Zlochower, Phys. Rev. D **77**, 101501 (2008); C. Lousto and Y. Zlochower, Phys. Rev. D **77**, 024034 (2008).
[54] E. Lorenz, Trans. N. Y Acad. Sci. **25**, 409 (1963); H. Poincaré, Les Méthodes nouvelles de la Mécanique Céleste. 3 volumes (1892). English translation, New Methods of Celestial Mechanics, History of Modern Physics and Astronomy 13, Amer. Inst. Phys. (1993); S. Jhingan, N. Dadhich and P. Joshi, Phys. Rev. D **63**, 044010 (2001).
[55] Y. Torigoe, K. Hattori, and H. Asada, Phys. Rev. Lett. **102**, 251101 (2009).
[56] S. Bai, Z. Cao, W.B. Han, C.Y. Lin, H.J. Yo and J.P. Yu, J. Phys: Conf. Ser. **330** 012016 (2011).
[57] Z. Cao, H.J. Yo, and J.P. Yu, Phys. Rev. D **78**, 124011 (2008).
[58] M. Parashar, http://nsfcac.rutgers.edu/TASSL/Projects/GrACE/.
[59] B. Brügmann, J. González, M. Hannam, S. Husa, U. Sperhake and W. Tichy, Phys. Rev. D **77**, 024027 (2008).
[60] T. Yamamoto, M. Shibata, and K. Taniguchi, Phys. Rev. D **78**, 064054 (2008).
[61] E. Schnetter, S. Hawley, and I. Hawke, Class. Quantum Grav. **21**, 1465 (2004).
[62] C. Bona, J. Masso, E. Seidel, and J. Stela, Phys. Rev. Lett., **75**, 600 (1995).
[63] M. Alcubierre *et al*, Phys. Rev. D **67**, 084023 (2003).

[64] E. Gourgoulhon, P. Grandclément, K. Taniguchi, J. Marck, and S. Bonazzola, Phys. Rev. D **63**, 064029 (2001); K. Taniguchi and E. Gourgoulhon, Phys. Rev. D **66**, 104019 (2002); ibid. **68**, 124025 (2003).
[65] http://www.lorene.obspm.fr/.
[66] G.B. Cook, Living Rev. Relativity **3**, 5 (2000); E. Gourgoulhon, J. Phys.: Conf. Ser. **91**, 012001 (2007).
[67] J.M. Bowen and J.W. York, Phys. Rev. D **21**, 2047 (1980).
[68] D.R. Brill and R.W. Lindquist, Phys. Rev. **131**, 471 (1963).
[69] S. Brandt and B. Brügmann, Phys. Rev. Lett. **78**, 3606 (1997).
[70] S. Bonazzola, E. Gourgoulhon, J.A. Marck, Phys. Rev. D **58**, 104020 (1998).
[71] M. Ansorg, B. Brug̈mann, and W. Tichy, Phys. Rev. D **70**, 064011 (2004).
[72] E. Gourgoulhon, P. Grandclément, and S. Bonazzola, Phys. Rev. D **65**, 044020 (2002); P. Grandclément, E. Gourgoulhon, and S. Bonazzola, Phys. Rev. D **65**, 044021 (2002).
[73] J.P. Boyd, Chebyshev and Fourier Spectral Methods, Dover Publications (2001).
[74] W. Tichy and B. Bruegmann, Phys. Rev. D **69**, 024006 (2004).
[75] M. Shibata and T. Nakamura, Phys. Rev. D **52**, 5428 (1995).
[76] M. Ruiz, M. Alcubierre, D. Nunez, and R. Takahashi, Gen. Rel. Grav. **40**, 2467 (2008).
[77] The gravitational background effect depends in the perturbative regime only on the ratio m_3/R. The ratio m_3/R in our simulation is in the range $m_3/R \in [0.001, 0.1]$, which is much larger than the ones in the usual astrophysical cases. Thus our result can be applied straightforwardly to those usual cases. However, it is quite possible for the existence of BBH systems near the center of a galaxy where m_3/R would be larger than in the usual astrophysical cases by several orders of magnitude. Our study should be also applicable to such cases as long as the ratio m_3/R's are comparable.
[78] In Fig. 5d, there is a gap between the measured proper time and the direct sum of the estimated proper merging time and the proper propagation time. The estimated proper merging time is defined here as the time for the nearest proper distance between two BH's apparent horizons becoming zero. The measured proper time is for the highest peak of the gravitational wave to arrive at the detector. The highest peak of gravitational wave should happen when the two BHs *really* merge, and thus later than the estimated proper merging time. This explains the gap.
[79] P.C. Peters, Phys. Rev. **136**, B1224 (1964).
[80] C.W. Lincoln and C.M. Will, Phys. Rev. D **42**, 1123 (1990).
[81] The separation of the BBH can not increase indefinitely under the assumption in this work. When the separation is comparable with R, the whole configuration turns to a three-body problem to which the perturbational method in this work cannot apply.